Determining the rotational period distribution of the icy cores of Jupiter-family comets in comparison to other small solar system bodies

The University of Kent

School of Physical Science

Tilo Hohenschläger, th202@kent.ac.uk

ABSTRACT

The main object of this project was the accumulation and in depth evaluation of already published data concerning Jupiter-Family Comets, Centaurs, and Kuiper Belt Objects concentrating on the rotational period and their distribution in order to find statistical correlations. We undertook an extensive search of published data in regards to the rotational period and axial ratio, a/b, of these objects. For this we used the SAO/NASA Astrophysics Data system (ADS). Our findings are within the agreement of the proposed rubble pile model and underline the evolutional connection between the transneptunian objects, Centaurs and JFCs. Much work has still to be done, since the review of the data incorporates only a small fraction of objects in question. Many new efforts are under way or in the planning stage to increase the data available that will allows us to increase our understanding of the small solar system bodies.

TABLE OF CONTENT

1. INTRODUCTION

Astronomy, one of the oldest Sciences has captured the fascination of mankind throughout history and will probably do so for the unforeseen future. For millennia our ancestors looked up into the night sky in wonder, and now we have reached the technological ability to explore our solar system and the universe itself. One of the many captivating objects to study are Comets and their Nuclei because cometary nuclei are the most primitive observable objects remaining from the era of planetary formation.

1.1 Motivation for studying the planetary small body population

The impulse for investigating cometary nuclei especially Jupiter-Family comets (JFCs) comes from the fact that Comets can supply information about the formation, evolution and thermal history of our Solar System. Recognising the physical, compositional, and dynamical features of comets is necessary to understand how our solar system was formed, its evolution, and how it will evolve in the future. As *Weidenschilling* (2004) pointed out, comets are probably the least-altered objects surviving from the origin of the solar system. From their chemistry much can be learned about their formation. They also provide a unique record of the physical processes involved in their accretion. Original material from the solar nebula, probably a mixture of surviving interstellar grains and nebular condensates are now present in any comet. In addition, analogous studies of cometary nuclei and dynamically related objects should provide knowledge of their physical and collisional histories. Cometary nuclei have also affected the formation and evolution of planetary atmospheres and were sources of water and organic material to the terrestrial planets. Furthermore, cometary nuclei contribute to the Earth impact hazard and studying them will determine procedures for hazard mitigation in a predicted collision event. (*Lamy et al.*, 2004)

1.2 Classification of Comets, Centaurs, and Kuiper Belt Objects

Jupiter-Family Comets (JFC's) are defined as short period comets with orbital periods of ≤ 20 years, low inclination, direct orbits, and a Tisserand Parameter of $2 < T_j < 3$. The Tisserand Parameter with respect to Jupiter (T_j) is defined as follow

$$T_j = \frac{a_j}{a} + 2\left((1-e^2)\frac{a}{a_j}\right)^{1/2}\cos(i) \qquad (1)$$

and relates the orbital semi major axis of Jupiter (a_j) with the orbital semi major axis (a), eccentricity (e), and inclination (i) of the comet. This parameter is conserved in the circular, restricted three-body problem and provides a measure of the relative velocity of approach to Jupiter (*Jewitt*, 2004). Solar system dynamics studies by *Levison and Duncan* (1994) found that JFCs are a dynamically distinct group in which over 92% remain in the same dynamical class of the Tisserand family during the computer simulations. Later solar system dynamics studies showed that the scattered disk objects (SDOs) are the probable source for the JFCs (*Duncan and Levison,* 1997) but *Volk and Malhotra* (2008) only

partially agree. They argue that the SDOs are not the sole source for the JFCs and that alternative sources in the classical Kuiper belt objects and Jupiter Trojans may exist. Other Comet groups include Long Period Comets (LPC's) with an orbital period of > 200 years and a random orbital inclination due to their origin from the Oort cloud. Halley-Family Comets (HFCs) have orbital periods of 20 – 200 years and the same orbital inclination as the planets, with a Tisserand Parameter T_j < 2 (*Lowry et al.,* 2008). Comets with T_j > 3 and an orbital semimajor axis a < a_j are designated as Encke-type comets. Chiron-type or Centaurs are classified by having a Tisserand Parameter T_j > 3 and a > a_j implying an orbit which is exterior to Jupiter (*Duncan et al.*, 2004). Edgeworth and Kuiper predicted the existence of a belt of small bodies beyond Neptune, which is known today as the Kuiper Belt. The transneptunian population is usually divided in two subpopulations, the scattered disk and the Kuiper Belt. In principle, objects which do not suffer close encounters with Neptune and do not undergo macroscopic migration in semimajor axis can be classified as the Kuiper Belt objects. On the contrary, objects that are transported in semimajor axis by close and distant encounters with Neptune would constitute the scattered disk (*Morbidelli and Brown*, 2004). Figures 13 to 15 in the appendix show the orbit diagrams of the 3 classes of celestial bodies discussed for better visualisation purposes.

1.3 Structure of cometary nuclei

As we will see, the rotational period of a comet is restricted by its internal structure and its density. Various models of structural compositions have been proposed over the last decades and Figure 1 shows a collection of them. Figure 1(a) depicts the icy conglomerate model suggested by Whipple. It envisages the comets nucleus as a single macroscopic mixture of volatile ices and meteoric material. With this model Whipple tried to explain the non-gravitational motion of periodic comets suggesting a "rocket effect" from sublimating ices on the surface of the rotating nucleus (*Weissman et al.*, 2004). Figure 1(b) and (c) shows the fractal aggregate model of Donn et al. and the primordial rubble pile model of Weissman respectively. The models have in common that the cometary nuclei are aggregates of smaller icy planetesimals loosely bound in a random fashion. These two models could explain observed processes like splitting and outbursts and could provide explanations of irregular activity on the surfaces of the nuclei (*Weissman et al.*, 2004). Figure 1(d) proposes a model called the "icy-glue model". This model was only conceived after the Spacecraft mission flybys of Comet 1/P Halley in 1986 by Gombosi and Houpis. The model advocates that comets are composed of porous refractory boulders with a composition similar to the outer main-belt asteroids, cemented together by icy-conglomerate glue. This model was created to explain the irregular topography seen in the Giotto Spacecraft images as well as the collimated jets emanating from the surface (*Weissman et al.*, 2004). Evidence given in Section 4 is pointing in the direction of the fluffy-aggregate and primordial rubble-pile models.

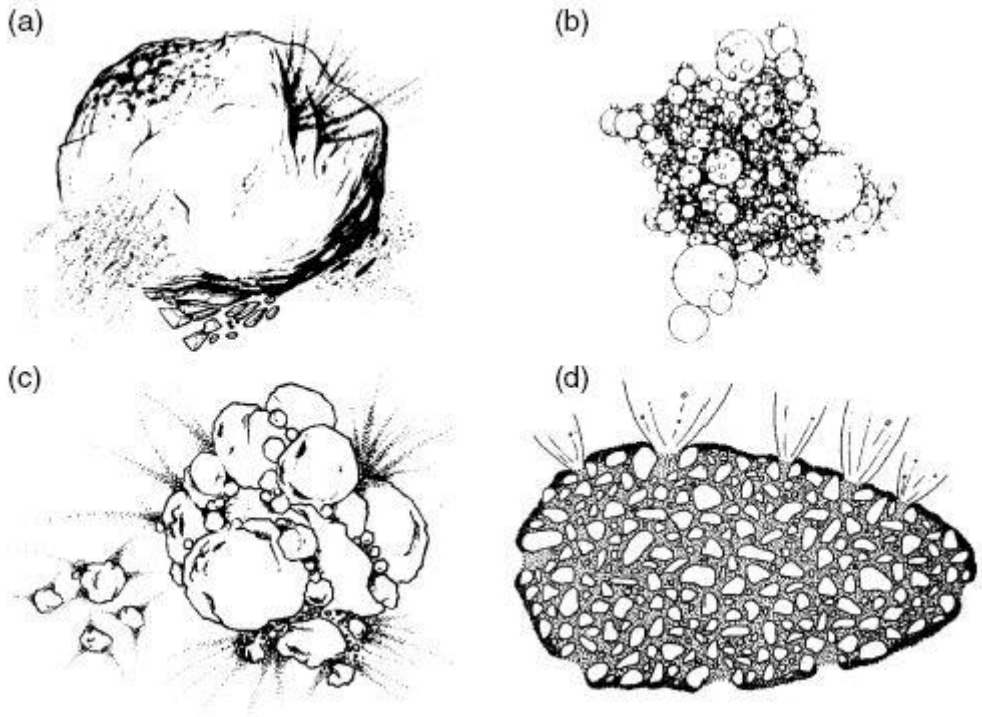

Figure 1: Artists concepts of various models for cometary nuclei. Adapted from *Weissman et al.* (2004)

1.4 Focus of the project and future perspective

The projects focus is the accumulation and in depth evaluation of already published data concerning JFCs, Centaurs, and KBOs concentrating on the rotational period and their distribution in order to find statistical correlations. To accomplish this, we undertook an extensive search to collect published data on the rotational period and axial ratio, a/b, of cometary nuclei, Centaurs, and Kuiper Belt Objects. The collection of these objects radii for evaluation of the size distribution and any correlation within was proposed, but time constraints dictated that this aspect be excluded from this work. All data mining was carried out using the digital library of the Smithsonian Astrophysical Observatory (SAO) and the National Aeronautics and Space Administration (NASA), SAO/NASA Astrophysics Data system (ADS). This is available online at http://adsabs.harvard.edu/index.html.

Figure 2 (*Jewitt*, 2004*)* shows the current interrelations between the planetary small body populations. Comparing the rotational period of comets can reveal answers about their composition and internal structure and may help to erase these question marks in Figure 2.

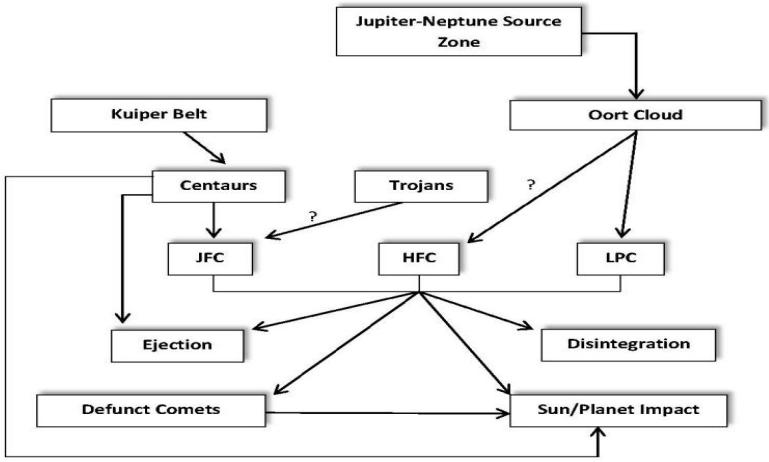

Figure 2: Current interrelations among the planetary small body populations. Question marks indicate the uncertain path from the Oort cloud to the HFCs and the unknown contribution to the JFCs from the Trojans of the giant planets. The defunct comets include both dead (totally devolatilized) and dormant (volatiles shielded from solar insolation) bodies. Adapted from *Jewitt and Fernández* (2001)

The Survey of Ensemble Physical Properties of Cometary Nuclei (SEPPCoN) is a study to collect data about the distribution of JFCs size, shape, spin-rate, albedo and surface composition through thermal IR imaging from NASA`s Spitzer Space Telescope at wavelengths of 16-22 μm and optical imaging at wavelengths of 400-700 nm with telescopes like the European Southern Observatory`s 8.2m VLT array in Chile or the 10m Keck Telescope in Hawaii and many more. This survey is an on-going effort and more results are eagerly awaited. This links in with the Rosetta Spacecraft Mission of the European Space Agency (ESA), to the comet 67P/Churyumov-Gerasimenko arriving in 2014. While writing this report the Japanese Aerospace Exploration Agency (JAXA) also announced that government officials gave the go ahead for a new robotic exploration and sample return mission to the near-Earth asteroid 1999 JU3, which is due for Launch in 2014. All these endeavours will greatly advance our understanding of the small body population in our solar system and will ensure high quality science in the decades to come.

2. METHOD

2.1 Observational Techniques for determination of the rotational period and axis ratio used in this project

2.11 Use of reflected light

Cometary nuclei are some of the most difficult objects of the Solar System to observe. The reason for this is that they are either bright and hidden by a coma when near to Earth or they are very faint and less active when and far from the Sun. Nonetheless multiple observational techniques have been devised which include ground based visible-wavelength imaging, thermal IR detection, radar

and spacecraft observations. The main observational technique is ground based optical photometry utilising the detection of solar light reflected by the comets nucleus. Best results are usually achieved observing the comet near aphelion. However this remains problematic since large heliocentric distances (r_h) and geocentric distances (Δ) usually result in very faint signals and the criterion used to decide the nonexistence of a coma, namely the stellar appearance of the nucleus, can introduce an unresolved coma that contaminates the observed signal. Inadequate spatial resolution observing at these large distances makes accounting for the coma contribution of the nucleus difficult and limits observations to snapshots, but in some cases multiple datasets have been recorded that allow the construction of a light curve. A light curve supplies information on the shape and the rotational period of the cometary nucleus. So far only optical (reflected light) and infrared (thermal emissions) observations are permitting the construction of such light curves. In these, the periodic temporal variation of the brightness is interpreted in terms of the rotation of an elongated body (*Lamy et al.*, 2004). Various methods have been devised to calculate the rotational period but for the data obtained in this study the two most common used period-detection techniques used, were the Lomb method and the Harris method. The increased complexity of the spectrum of astronomical observations that is non-uniform leads to the difficulty of finding an unambiguously defined period (*Lomb*, 1976). The Lomb method uses in essence a modified version of a Fourier spectral analysis but accounts for the fact that the data are unevenly spaced and therefore the spectral power is normalized. The consequence is that the emphasis of the data rests on a "per point" basis instead of a "per time" interval basis. The Lomb-normalised spectral power as a function of frequency $P_N(\omega)$ is given as

$$P_N(\omega) = \frac{1}{2\sigma^2}\frac{\left[\sum_j (h_j - \bar{h})\cos\omega\,(t_j - \tau)\right]^2}{\sum_j cos^2\omega\,(t_j - \tau)} + \frac{\left[\sum_j (h_j - \bar{h})sin\omega\,(t_j - \tau)\right]^2}{\sum_j sin^2\omega\,(t_j - \tau)} \quad (2)$$

where ω is the angular frequency, also 2πf, σ^2 is the variance of the data, $\bar{h}$ is the mean of the measurements, h_j and t_j are the measurements and their times, and τ is an offset that makes $P_N(\omega)$ independent of shifting all the t_i by any constant. τ is defined as

$$\tan(2\omega\tau) = \frac{\sum_j sin2\omega t_j}{\sum_j cos2\omega t_j} \quad (3)$$

With this method the best period is the one that maximises the normalised spectral power (*Sheppard S. S., Lacerda P., and Ortiz J. L.*, 2008).

The Harris method was developed for studies of asteroid light curves and is primarily a fit of the data to a Fourier series and is determined as

$$H(\alpha,t) = \bar{H}(\alpha) + \sum_{l=1}^{m} A_1 sin\frac{2\pi l}{P}(t - t_0) + B_1 cos\frac{2\pi l}{P}(t - t_0) \quad (4)$$

where H($\boldsymbol{\alpha}$,*t*) is the computed magnitude at solar phase angle $\boldsymbol{\alpha}$ and time t, $\bar{H}(\boldsymbol{\alpha})$ is the mean magnitude at phase angle $\boldsymbol{\alpha}$ and A_1 and B_1 are Fourier coefficients. For a given period P, the fit is carried out by finding the minimum of a bias-corrected variance

$$s^2 = \frac{1}{n-k}\sum_{i=1}^{n}\left(\frac{\delta_i}{\varepsilon_i}\right)^2 \quad (5)$$

where $\delta_i = V_i(\alpha_j) - H(\alpha_j, t_i)$ is the deviation from the observations to the model, with α_j the phase angle of night j and ε_i are a priori error estimates of the measurement. K is defined as k = 2m + p+ 1, where m is the degree of the Fourier series and p is the total number of days of data. The minimum value of s^2 corresponds to the best solution found (*Sheppard S. S., Lacerda P., and Ortiz J. L.*, 2008).

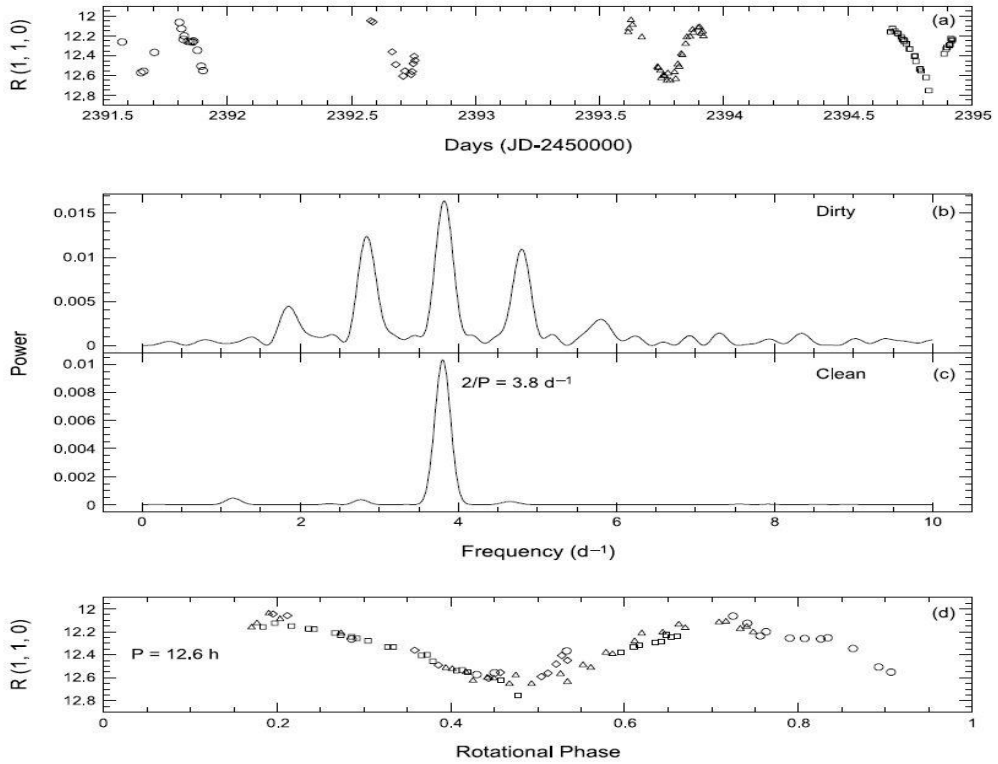

Figure 3: (top) Example of Lightcurve data, in this case of Comet 28P/Neujmin1, in the R filter as a function of time in terms of Julian days (JD). (centre) Fourier power spectrum corresponding to the data and after applying clean algorithm. (bottom) Rotationally phased Lightcurve data for the rotation period of 12.6h. (*Samarasinha et al*. 2004)

Figure 3 shows an example how a rotational period for a comet can be obtained using mathematical operations as described before. The amplitude of such a Lightcurve yields the axis ratio, a/b, if it is possible to independently constrain the orientation of the spin axis. It is assumed that the brightness variations are purely shape induced and is not caused through variations of the albedo of the nucleus surface. This can be modelled as a prolate spheroid with semimajor axis a, and semiminor axis b and c, where a > b and b = c. Figure 4 shows a prolate spheroid model and Figure 5 shows the model of the nucleus of Comet 19P/Borrelly derived from the Hubble Space Telescope (HST) observations made in 1994, as the overlaid spheroid, and validated by images taken of the Deep Space 1 spacecraft (*Lamy et al.*, 2004)

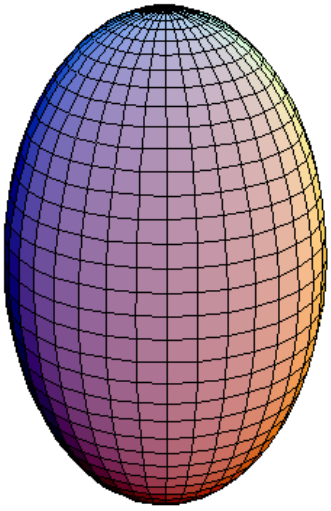

Figure 4: Prolate Spheroid [1]

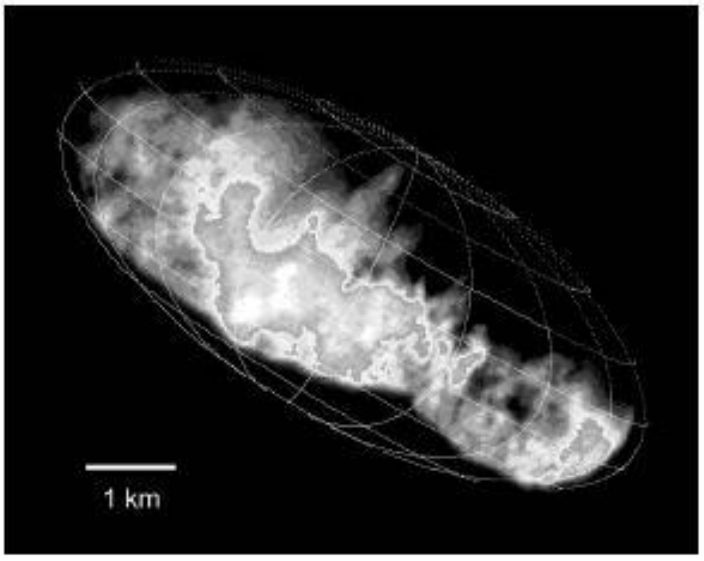

Figure 5: The prolate spheroid model of the nucleus of Comet 19P/Borrelly derived from the HST observations made in 1994 is verified by the best in situ image taken by the Deep Space 1 spacecraft in 2001. Adapted from *Lamy et al.* (2004)

A lower limit of the axial ratio can also be estimated using

$$\frac{a}{b} = 10^{0.4\,\Delta m} \tag{6}$$

where Δm is the range of the observed magnitudes (*Weissman et al.*, 2004). Using thermal infrared emissions for attaining a lightcurve, the non-homogeneous two-dimensional temperature distribution over the surface will be of importance. Non-spherical thermal modelling by Brown predicts larger amplitudes of the lightcurve in the infrared than in the visible light, an effect supposedly observed on the comet 10P/Tempel 2. However these interpretations are valid only for simple spheroidal models and more complex configurations and effects such as shadowing and un-illuminated areas can yet not be dealt with accurately (*Lamy et al.*, 2004).

2.12 Radar observations

Radio Detection and Ranging (Radar) uses radiation of electromagnetic waves against the target in question and extracts information about it through the analysis of the returned echo. Radar observations of cometary nuclei are sparse due to the rarity of close comet approaches to Earth. A radar signal sent from Earth will start to spread out as soon as it is send. The more distant the object is, the more spread out the beam will be when it arrives at the target and the more spread out the echo will be when received. This will result in a very weak signal received. This is called Δ^{-4} dependency for detectability of comets and makes detailed imaging unfeasible at distances much greater than 0.10 Astronomical Units (AU) (*Harmon J. K. and Nolan M. C.*, 2005). However radar observations have been achieved for comets like 103P/Hartley 2, P/2005 JQ5 or 2P/Encke as well as others. Observations of these comets were achieved by using the Arecibo 305 m

Radio Telescopes S-band radar with a frequency of 2380 MHz, which corresponds to a wavelength of λ = 12.6 cm. Uses of other radar systems such as the Goldstone S-band, λ =12.9 cm, or Goldstone X-band, λ = 3.5 cm have been reported (*Harmon et al.*, 2004). To attain a Doppler spectrum an unmodulated (monochromatic) wave is transmitted and a Doppler-broadened echo will be received. After a computational analysis of the received signals power spectrum a spike should stick out of the background noise (*Harmon et al.*, 2004).

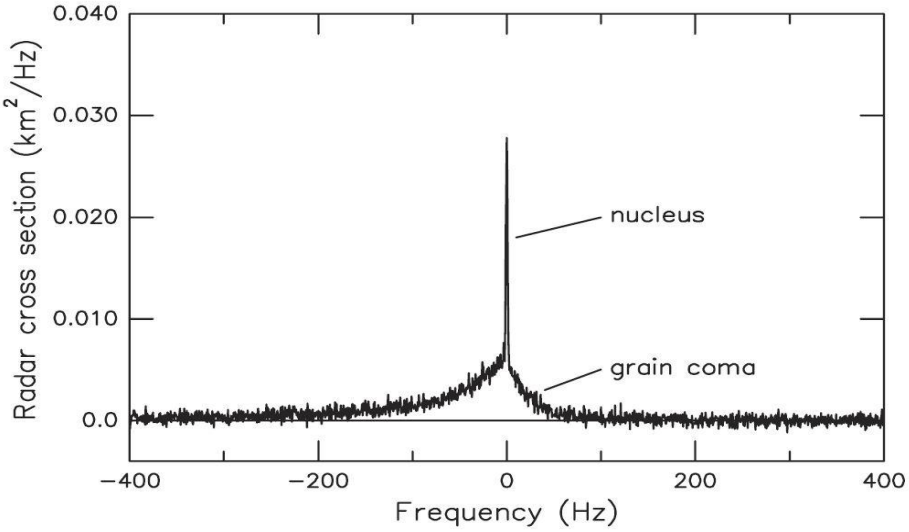

Figure 6: Radar Doppler spectrum (OC polarization) of Comet 103P/Hartley 2, with narrow nucleus and broad grain-coma components denoted. Adapted from *Harmon et al.* (2011)

Figure 6 shows an example of such a spectrum. The Doppler spreading of the nucleus represents the radial velocity spread from the apparent rotation of the nucleus. The most fundamental radar parameter measured from the returned echo is the radar cross section σ. This can be calculated using

$$\sigma = \frac{(4\,\pi\,)^3\,\Delta^4\,P_r}{P_t\,G^2\,\lambda^2} \tag{7}$$

where Δ is the comet distance, P_t is the transmitted power, P_r is the echo power and $G = 4\,\boldsymbol{\pi}\,A_e / \lambda^2$ is the beam gain of the radar antenna of the effective area A_e. In the case that the size of the nucleus is known, the geometric radar albedo can be found through normalisation of σ. This can then be used for surface density estimates (*Harmon et al.,* 2004).

2.13 Spacecraft observations

As mentioned in chapter 2.11 observing small cometary nuclei with ground based telescopes can be difficult. To study those bodies in detail and from a close range it is necessary to utilise dedicated spacecrafts. In 1985 the International Sun Earth Explorer 3 (ISEE 3), renamed after its first mission objective was completed to International Cometary Explorer (ICE), traversed the plasma tail of Comet 21P/Giacobini-Zinner to study the

interaction between the solar wind and the cometary atmosphere. 1986 it also transited between the Sun and Comet 1P/Halley (*National Space Science Data Center*, 2012). 1986 saw a fleet of space probes being sent to pass Comet 1P/Halley. While the 2 Japanese probes, Sakegaki and Suisei, did not carry experiments for studying the nucleus, the Vega 1 and 2 probes as well as Giotto, carried sophisticated remote sensing experiments for studying the nucleus (*Keller et al.*, 2004). Even after being damaged during 1P/Halley's flyby, most of Giotto's instruments remained operational and it was decided to extend the mission. In 1992 the space probe encountered 26P/Grigg-Skjellerup (*Science Programme European Space Agency*, 2003). Deep Space 1, which was developed as a technology demonstration probe, was launched 1998 to fly by a near-Earth asteroid in 1999 and its mission was extended to fly by Comet 19P/Borrelly. The spacecraft carried the Miniature Integrated Camera Spectrometer (MICAS) which combines two visible channels with UV and IR spectrometers to study the chemical composition, geomorphology, size, spin-state, and atmosphere of the asteroid and comet (*National Space Science Data Center*, 2012). In 1999 the Stardust probe was sent to the Comet 81P/Wild 2. It contained a Sample Return Capsule (SRC) to collect particles of dust and volatiles from the comets coma and interstellar particles. In 2002 the space probe flew past the asteroid 5535 Annefrank and imaged it. In the year 2003/2004 it encountered Comet 81P/Wild 2 to collect samples and image the comets surface. The SRC was returned to Earth for analysis in 2006. After funding was secured the Stardust mission was extended and renamed as the New Exploration of Tempel 1 (NExT) mission. Comet 9P/Tempel 1 was the target of the Deep Impact Mission in 2005, which delivered an impactor into the surface of the comet. Stardust/NExT did its fly by in February 2011 and was looking for signs of cater modification and extended the mapping of the nucleus (*National Space Science Data Center*, 2012). The Deep Impact spacecraft was launched in 2005 and as previously mentioned delivered a projectile which struck the surface of the comet on the sunlit side of the nucleus with a velocity of 10.2 km/s and impact energy of $19x10^9$ Joules, which vaporised the impactor and much of the ejecta. The fly by spacecraft was approximately 10,000 km away and imaged the whole process. This mission also got an extension which had 2 parts. The Deep Impact Extended Investigation (DIXI) involved flying by Comet 103P/Hartley 2 in 2010 for imaging and data collection purposes. The Extrasolar Planet Observation and Characterisation (EPOCh) mission used the probes imaging system to observe nearby bright stars with known large planets to characterize them and search for new candidates. These two extended missions together are known as EPOXI (*National Space Science Data Center*, 2012). The Rosetta Spacecraft was launched in 2004 and is currently on its way to the Comet 67P/Churyumov-Gerasimenko. So far it has managed a flyby of asteroid 2867 Stein in 2008 and asteroid 21 Lutetia in 2010. The probe is scheduled to arrive at the Comet 67P in 2014 and deliver the Philae Lander to the surface of the comet for analysis of the comets nucleus (*National Space Science Data Center*, 2012).

Other observations are contributed by space bound observatories like the HST, Spitzer Space Telescope, the Solar and Heliospheric Observatory (SOHO) and the Chandra X-ray Observatory. Observing in different wavelengths and without Earth's atmospheric conditions complicating imaging, the quality of data received is greatly improved.

3. RESULTS

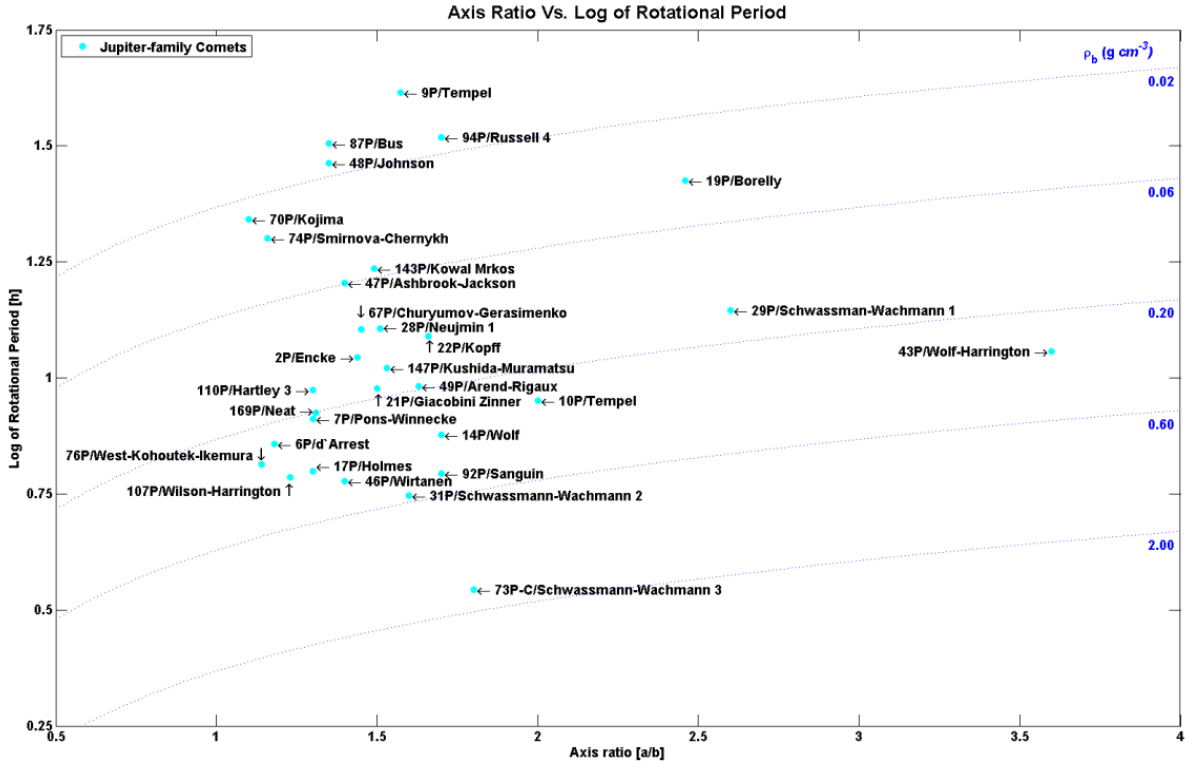

Figure 7: Rotation Periods and axial ratios, a/b, for 30 Jupiter-family comets and 1 Halley-type comet. Their inferred density lower limits are given by their position on this plot. Constant-density curves for values of 0.02, 0.06, 0.2, 0.6, and 2.0 g cm^{-3} have been overplotted for comparison. Please see reference section for data references.

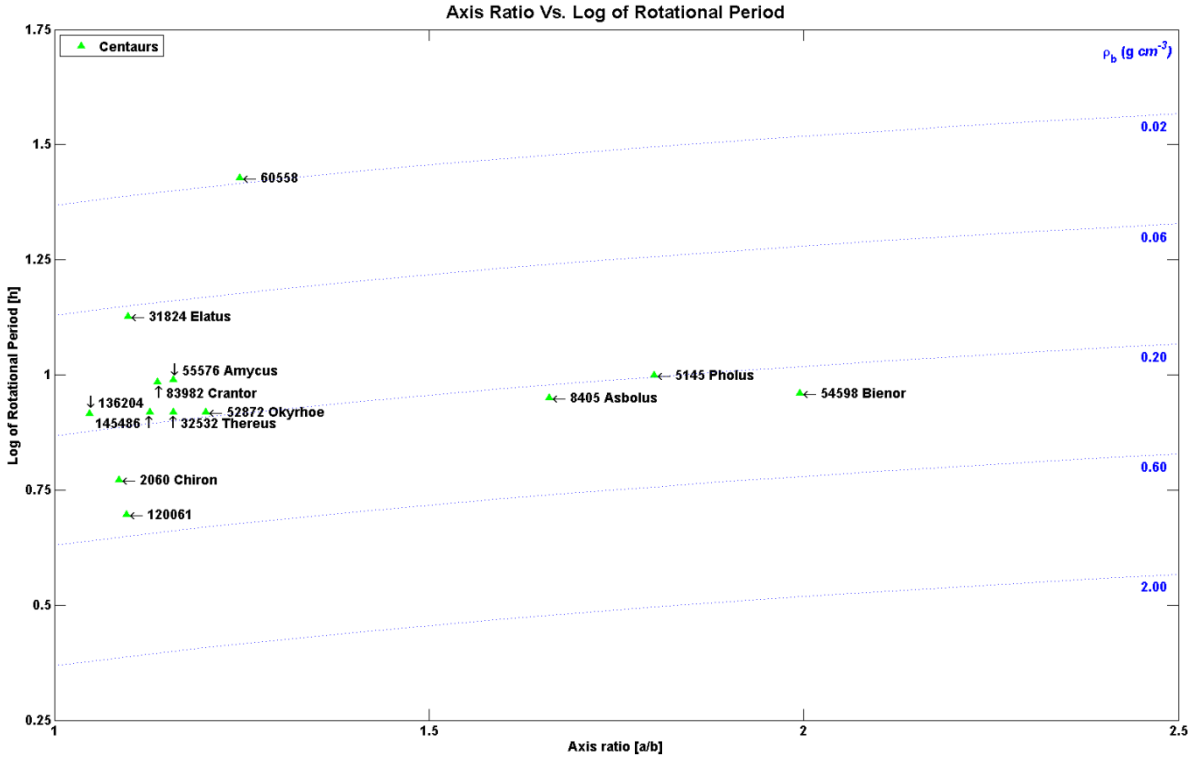

Figure 8: Rotation Periods and axial ratios, a/b, for 13 Centaurs. Their inferred density lower limits are given by their position on this plot. Constant-density curves for values of 0.02, 0.06, 0.2, 0.6, and 2.0 g cm^{-3} have been overplotted for comparison. Please see reference section for data references.

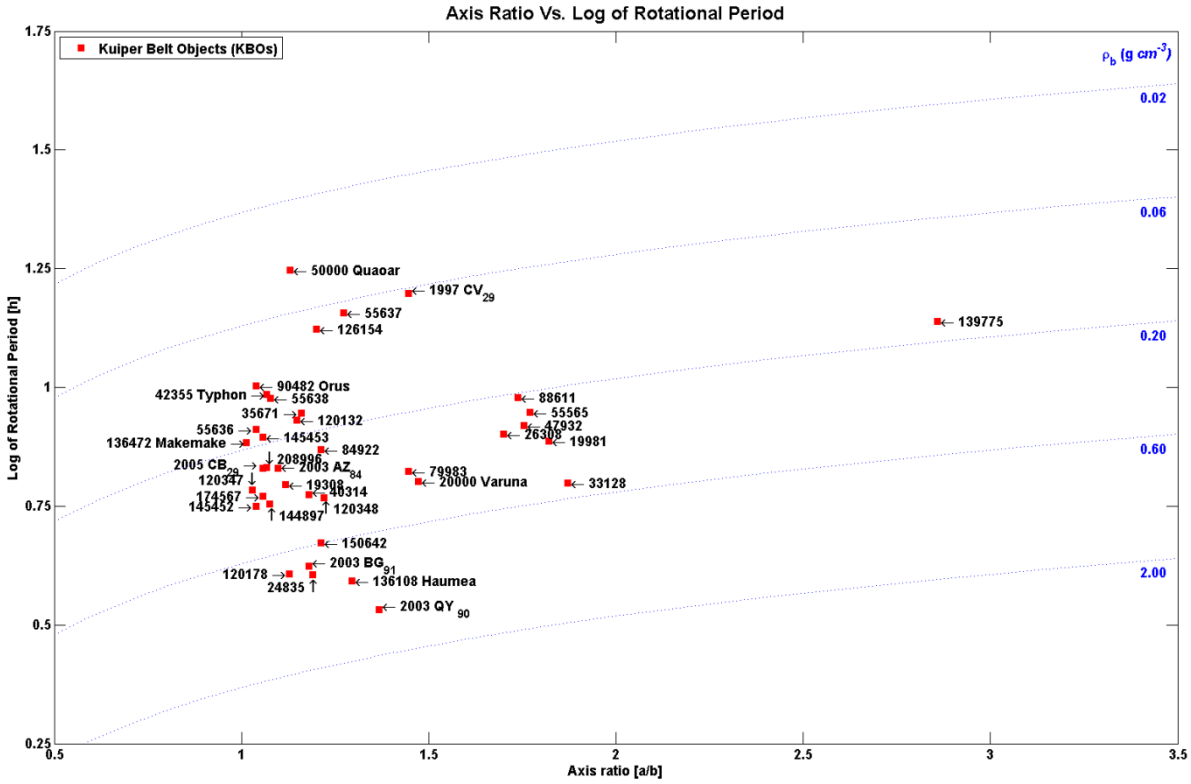

Figure 9: Rotation Periods and axial ratios, a/b, for 39 Kuiper Belt Objects (KBOs). Their inferred density lower limits are given by their position on this plot. Constant-density curves for values of 0.02, 0.06, 0.2, 0.6, and 2.0 g cm^{-3} have been overplotted for comparison. Please see reference section for data references.

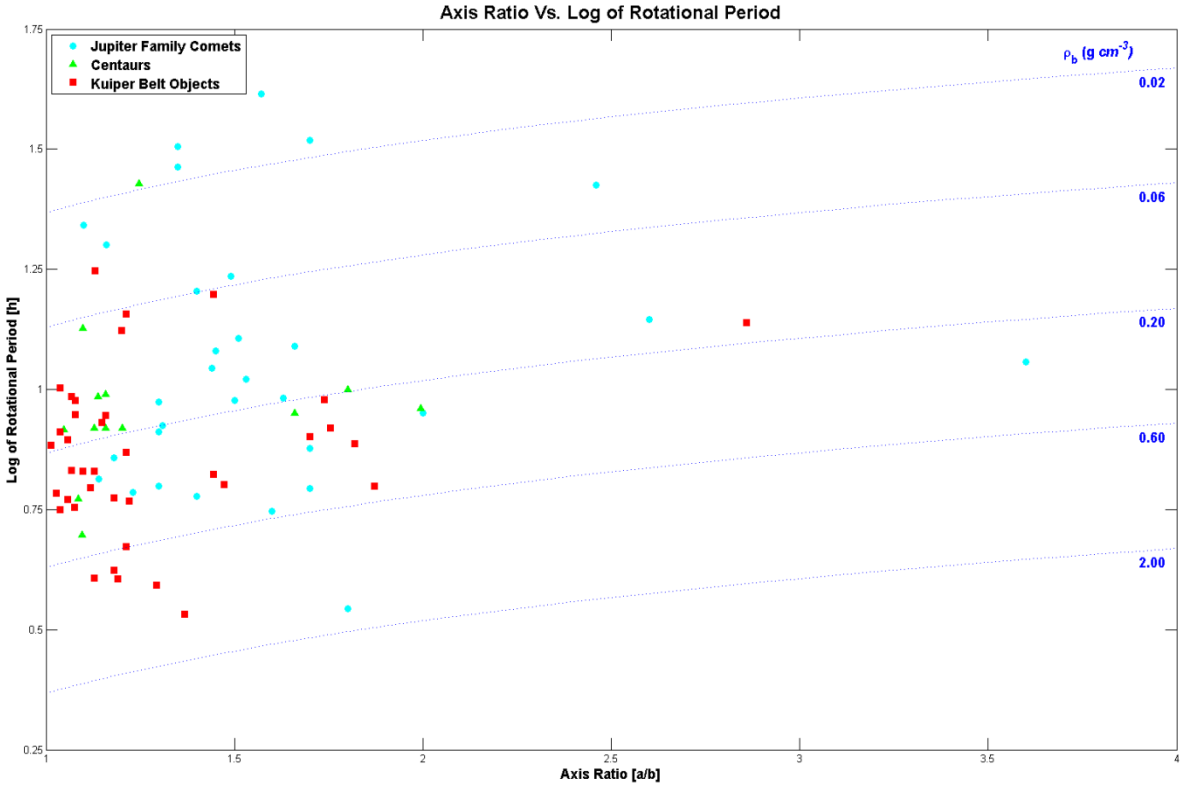

Figure 10: Rotation Periods and axial ratios, a/b, for the three groups overlaid. Their inferred density lower limits are given by their position on this plot. Constant-density curves for values of 0.02, 0.06, 0.2, 0.6, and 2.0 g cm^{-3} have been overplotted for comparison.

Figure 7 to 10 show the results of our data collecting efforts for three type of minor solar system body. Figure 7 depicts the class of Jupiter-Family comets, Figure 8 shows the class of Centaurs, while Figure 9 displays the KBO population. All data points in Figures 7 to 9 include name labels for identification purposes. In Figure 7 and 9 the x-axis extends on the left hand side to 0.5 for labelling data point reasons only, since an Axis ratio of < 1is meaningless. Figure 10 shows all 3 populations overlaid for analysis and interpretation. All graphs show the rotational period as the Log $_{10}$ of the actual measurement for the purpose of data handling and display. The rotation periods P_{rot} range from 3.4 to 41.27 h, while the projected axial ratios, a/b, range from 1.013 to 3.60. The bulk densities, D_N, for the JFCs, Centaurs and KBOs range from 0.010 to 1.602 g cm^{-3}. These were calculated using the following equation

$$D_N \leq \frac{10.9}{P_{rot}^2} \frac{a}{b} \tag{8}$$

where P_{rot} is in hours. These calculated parameters are only minima of the bulk density, because the axial ratio a/b is also only a minimum measurement due to the unknown orientation of the spin axis of the nuclei. Another reason is that the limit, which is calculated for the point where the gravitational forces balances the centripetal forces, does not necessarily mean that every comet is spinning at its fastest possible rate (*Snodgrass*, 2006). The constant-density curves for the values of 0.02, 0.06, 0.20, 0.60, and 2.00 g cm^{-3}, visible as the blue dashed lines, were calculated using the equation for the critical rotation period $P_{critical}$ from the following equation

$$P_{critical} = \frac{3.3\ h}{\sqrt{\rho}} \sqrt{\frac{a}{b}} \tag{9}$$

where ρ is the density and is expressed in g cm^{-3}. (*Pravec and Harris*, 2000)

4. DISCUSSION

Figure 10 is comparable with previous published data by *Lowry et al.* (2008, see their Fig.2) and *Weissman et al.* (2004, see their Fig.8). The rotation period vs. shape distributions overlap well for the majority of the samples. A trend is noted for Centaurs and KBOs having smaller axial ratios, a/b, then JFCs, which seem generally more elongated. This might be an observational bias because the known KBOs are much larger due to practical difficulties in observing distant KBOs with radius r < 50 km and hence are probably shaped under self-gravity (*Snodgrass*, 2006). *Lacerda and Luu* (2006) indicated that only KBOs with r < 200 km are particularly extended and having a minimum axial ratios of a/b < 2. Considering this, a larger number of smaller KBOs could have higher values for the axial ratio a/b, which have not been detected due to their extreme faintness. For the group of objects studied a density cutoff at ~ 0.6 g cm^{-3} is preeminent and corresponds to a 5.2 h rotational period. This suggests that the fastest rotating nuclei are stable against centrifugal disruption, if their bulk densities exceed ~ 0.6 g cm^{-3} (*Lamy et al.*, 2004 and *Weissman et al.*, 2004).

This cutoff density implies that comets are remarkable porous with porosity levels of ~ 70%. This suggests considerable macro porosity or large voids within the nucleus (*Snodgrass*, 2006). Snodgrass also points out the trend that the fastest rotating nuclei have lower values for a/b, which reflects the incapability of the rubble pile nuclei to maintain extended shapes. However a comparable spin-period cutoff was found by *Pravec and Harris* (2000) in their studies of asteroids. The accumulated data showed that a spin rate cutoff existed for a rotational period of 2.2 h and a bulk density of ~ 2-3 g cm^{-3} for near-Earth asteroids with a diameter D > 0.2 km. The lower value for the cutoff density in cometary nuclei indicates that comets are far less dense than asteroids, mainly due to their higher percentage of volatile content and/or more porous structure (*Snodgrass*, 2006). This phenomenon gives insight in to the structure and physical processes of cometary nuclei and other small solar system bodies. According to Pravec and Harris these results can be interpreted as evidence that these asteroids are loosely bound, gravity-dominated aggregates with negligible tensile strength. There is no reason why this should not be true in our case and we can therefore adapt the conclusion of the rubble-pile internal structure for the objects investigated here. A distinct group of asteroids with r < 150 m exists, which can spin faster than this limit, which are believed to be monolithic-rock fragments from possibly larger rubble-pile asteroids. This could certainly explain the fast spinning Fragment C of 73P/Schwassmann-Wachmann 3 with a measured P_{Rot}= 3.5 h. The calculated bulk density for the nucleus is D_N = 1.602 g cm^{-3}. Comet 73P/Schwassmann-Wachmann was observed in 1995 and outbursts were noted. A few months later the nucleus was observed again and multiple fragments of the parent comet were found. Since then many more fragments have been found. Other bodies that fall under the density cutoff are the following KBOs, 136108 Haumea, 24835, 150642, 2003 QY_{90}, 2003 BG_{91}, and 120178. For 24835 and 2003 QY_{90} observational bias might play a role in determination of the rotational period because of unresolved binary companions. However *Lowry et al.* (2008) stated that the existence of larger objects like 136108 Haumea does not rule out the rubble-pile structure of nuclei. The higher density of this object, with R ~ 1500 – 2500 km, can be explained by gravitational compression. This probably is also the explanation for the observed trend that Centaurs and KBOs have higher values for their bulk density than the JFCs. On the other hand *Holsapple* (2003) found that even a small cohesive strength of about 10^4 dynes cm^{-2} is enough to hold rotating elongated bodies together so that they can survive as rubble piles. Another indication for the rubble-pile nature comes from observations of splitting and disrupted comets. As Weisman et al. points out that there is no known mechanism for explaining random split events. A classic exemplar is the Jupiter-family comet 3D/Biela with an orbital period of 6.6 years, which was observed in the 18th and 19th century. In 1846 it was observed to split during apparition and returned in 1852 as a double comet. After that it was never seen again, but intense meteor showers were noted at the times the comet should have returned (*Weissman et al.*, 2004). Another more recent breakup event captured the attention of the astronomical community when fragments of the Jupiter-family comet, Shoemaker-Levy 9, plunged into the planet Jupiter. After using dynamical integration of the orbits of the comet backwards in time, it became apparent that Shoemaker-Levy 9 passed Jupiter at only 1.31 Jovian radii. This is inside of Jupiter`s Roche limit (*Weissman et al.*, 2004). The Roche limit is defined as the radius within which a

planet's tidal forces will overcome a celestial bodies gravitational self-attraction causing it to disintegrate. Figure 11 shows an image taken by the Hubble Space Telescope (HST) in May 1994. It shows a train of 21 fragments of the comet. It is notable that the brightest and therefore larger fragments are near the centre of the fragment chain. This was predicted by *Asphaug and Benz*, (1996) in their attempt to model the breakup of rubble pile structure. This is further evidence of why the rubble pile internal structure is favoured. Figure 12 shows a chain of impact craters on Jupiter's moon, Ganymede. This chain of craters was formed through a collision with 13 fragments, after the parent body broke apart by Jupiter's gravity. The scale similarity and the large central fragments were formed by impacts of chains of reassembled, virtually strengthless rubble piles of small icy planetesimals with similar bulk densities, which confirmed the previously stated models by Asphaug and Benz (*Weissman et al.*, 2004).

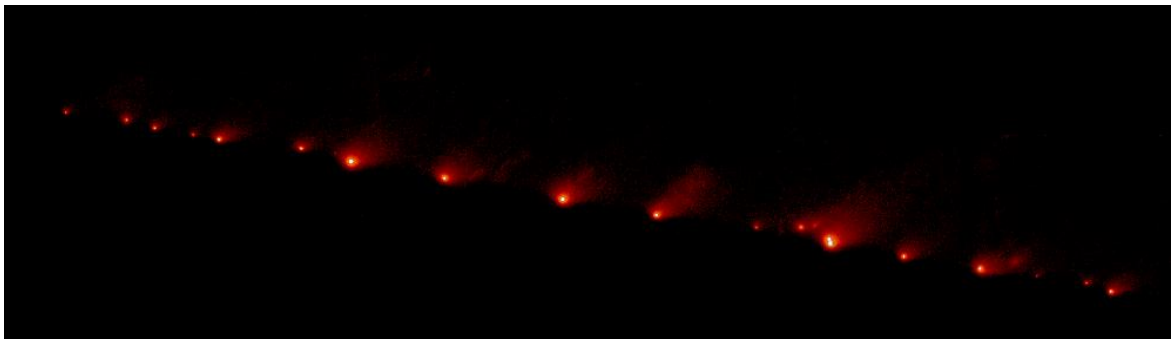

Figure 11: Image of the tidally disrupted comet Shoemaker-Levy 9. This Image was taken with the Wide Field Planetary Camera-2 (WFPC-2) of the Hubble Space Telescope on 17th May 1994. [2]

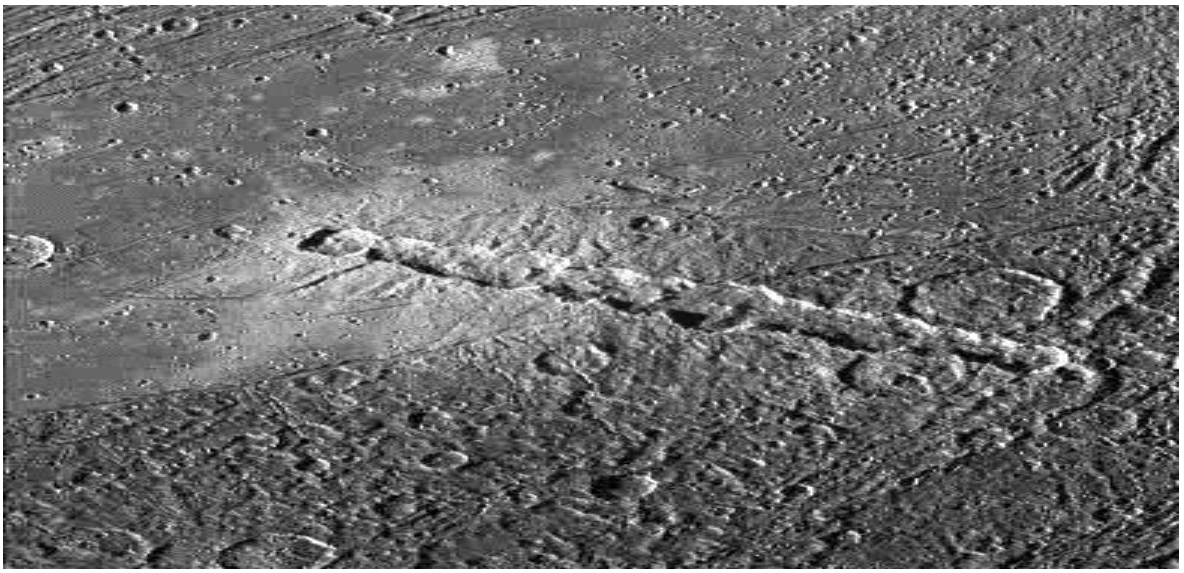

Figure 12: View of a chain of craters named Enki Catena on Jupiter`s moon, Ganymede.[3]

Spin states of cometary nuclei will alter during their life time for various reasons discussed next. Fortunately the time scales over which these changes occur are long and usually only little or no measurable changes in the rotational parameters occur (*Samarasinha et al.*, 2004).

However, several Comets have been reported to change their rotational state. Comet 2P/Encke, 9P/Tempel 1 and Comet C/1990 K1 was found to speed up, while Comet 10P/Tempel 2 was the first one detected to slow down (*Knight et al.*, 2011).

Outgassing of volatiles from the nucleus causes a reaction force on the nucleus. This not only changes the orbital motion of the comet, it also creates a torque on the nucleus and results in changes of its spin state. This process accounts for changes in the rotational state on a timescale as short as a single orbit.

Splitting events and changes to the moment of inertia because of mass loss are also mechanisms for changing the spin state of a comet. Regular mass loss of volatiles and dust through sublimation will cause changes on a much longer timescale than described before. Splitting events are stochastic in nature and a time scale for spin state alterations is uncertain, but likely larger than 100 years. Collisions with other objects are random events as well and certainly capable of changing the spin state. This is highly dependent on the orbit inclination of the body. Comets with low inclination like JFCs undergo more frequent collisions with other solar system objects than those with high inclination orbits. Tidal torques due to close encounters with other planets and the Sun also are also mechanisms for changing spin states. The differential gravitational potential experienced by different parts of the nucleus causes a net torque on the nucleus. This might be because of the tidal deformation of the nucleus or the shape (*Samarasinha et al*., 2004). Another mechanism for altering the spin state is the Yarkovsky-O'Keefe-Radzievskii-Paddack (YORP) effect. This describes a phenomenon where torque is produced due to both incident solar radiation pressure and the recoil effect from the anisotropic emissions of thermal photons. This effect was directly detected on a near-Earth asteroid (*Lowry et al*., 2008). In the previous mentioned case of Comet 10P/Tempel 2, tidal torqueing and splitting events have been dismissed and it was concluded that the decrease in spin rate was caused by outbursts (*Knight et al.*, 2011).

Approximately all observed properties of comets, including the changes of the spin states of cometary nuclei, are connected with their progressive disintegration. This can be regarded as the "aging" of a comet *(Meech K. J. and Svoreň J.*, 2004). This process can be divided in to four domains, the precometary phase, the accretion phase, the cold storage phase, and the active phase. In the precometary phase, the precursor cometary material, interstellar grains, is stored in the cold molecular clouds, of a temperature T = 10 K, and in warm, dense protostellar regions with T = 100 K. There the interstellar grains undergo significant processing by cosmic rays which create non-volatile material and highly reactive radicals. This material will then potentially be incorporated into the comets. In the accretion phase water ice that formed by low-pressure vapour deposition in the solar nebula will trap gases. This phase has significant implication for the chemical composition of comets because of temperature differences in the different forming regions. Oort cloud comets and LPs will have formed in the vicinity of the giant planets in a temperature environment of about 60 - 100 K, while KBOs formed and remained at temperatures of 30 - 50 K.

In the cold storage phase, comets might be stored for billions of years in the Oort cloud or the outer solar system, before passing close to the sun and become active. In this phase the outer layer of the comet gets radiated by galactic-cosmic rays, passing by stars, and supernovae events. While in the Oort cloud collisions might be rare, but objects ejected to the Oort cloud are probably heavy collisionally processed during their ejection. The active phase begins, when the comet enters the inner solar system *(Meech K. J. and Svoreň J.*, 2004). Numerical orbital integrations done by *Levison and Duncan* (1996) indicate that JFCs indeed come from the Kuiper Belt, which links to our findings of similar densities, rotational periods and axial ratios for the investigated population. They also point out that the physical lifetime of a JFC lies between 3000 and 30,000 years, with the most likely value of 12,000 years. This indicates that since JFCs are still being observed, a constant replenishment of the population is an on-going process. In fact it was suggested that the Centaurs are the observational connection between the KBOs and the JFCs (*Levison and Duncan*, 1996).

5. CONCLUSION

Our understanding of the solar system's small body population has been rapidly evolving thanks to the contribution from new technologies. Ground and space based observations in different wavelengths producing a wealth of data to synthesise ever closer models. In our project we looked into the distribution of the rotational periods of JFCs in order to find correlations between this distinct group and the Centaur and KBOs. Our findings are in agreement within the proposed rubble pile model and underline the evolutional connection between the transneptunian objects, Centaurs and JFCs. Much work is still needed, since the review of the data incorporates only a small fraction of objects in question. New efforts are currently under way or in the planning state, like the previously mentioned SEPPCoN project, the Rosetta Space Mission, Hayabusa 2, the Horizon Space probe and the observational program to study the YORP effect on the near-Earth asteroids. Especially the Rosetta Space Mission to Comet 67P/Churyumov-Gerasimenko will be an eagerly awaited highlight for the scientific community. With an extensive range of instruments on board, questions regarding the internal structure and composition will hopefully finally be answered.

ACKNOWLEDGEMENT

The author gratefully acknowledges the assistance of Dr. Stephen C. Lowry for his excellent supervision and my project partner Mr James Gardner in the area of data accumulation and presentation.

APPENDIX

Orbit visualisation of a Jupiter-family comet, a Centaur, and Kuiper Belt Object

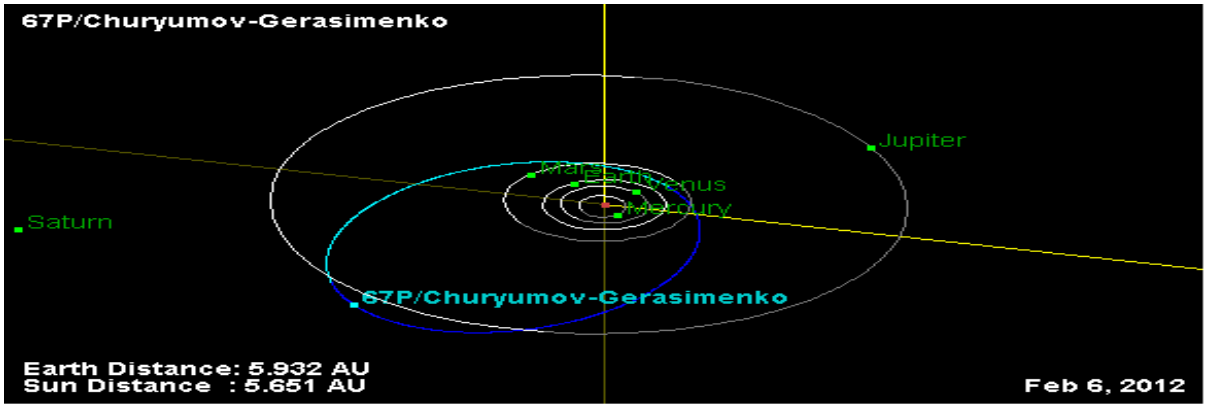

Figure 13: Orbit Diagram of Jupiter-family comet 67P/Churyumov-Gerasimenko [4]

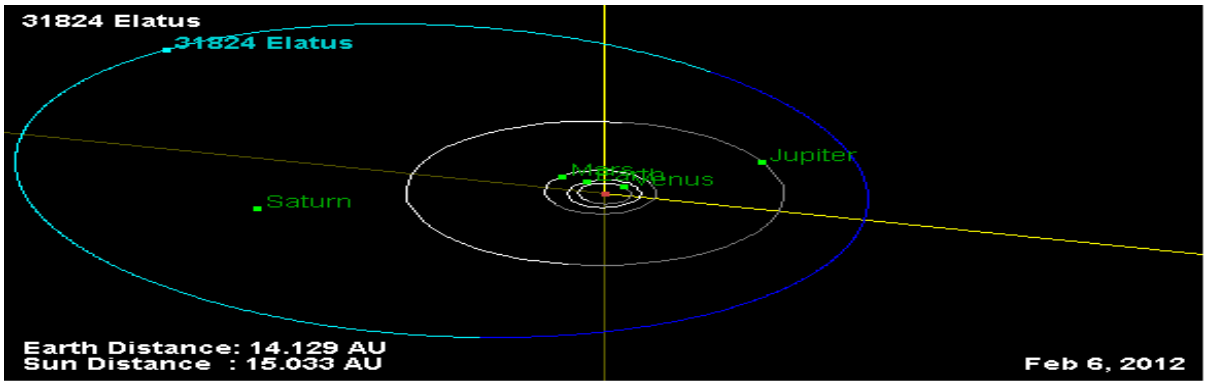

Figure 14: Orbit Diagram of the Centaur 31824 Elatus [5]

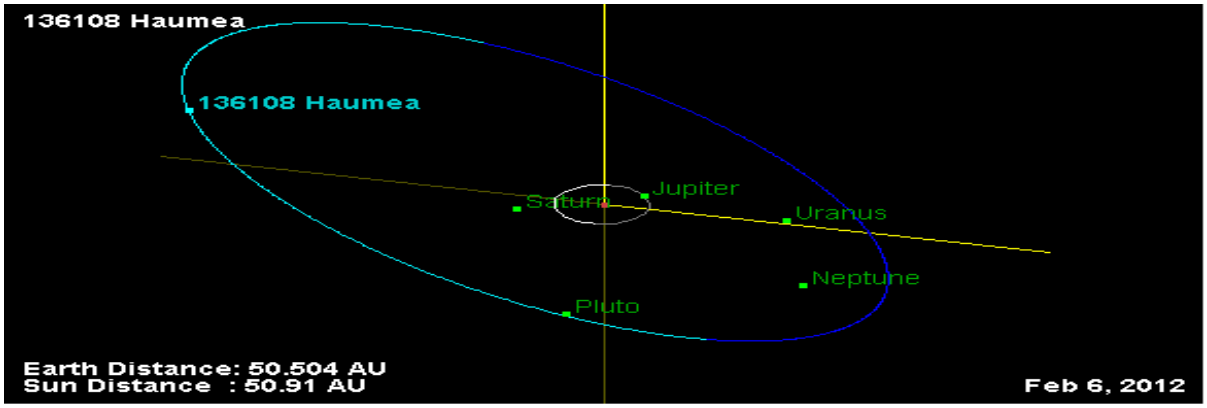

Figure 15: Orbit Diagram of the Kuiper Belt Object 136108 Haumea [6]

Table of Data

2P/Encke		
P_{rot} (h)	a/b	D_N (g cm^{-3})
11.083±0.003	**1.44**	**0.128**
(*Lowry and Weissman*, 2007)		
6P/d' Arrest		
P_{rot} (h)	a/b	D_N (g cm^{-3})
7.20±0.12	**1.18±0.08**	**0.248**
(*Lowry and Weissman*, 2003)		
7P/Pons-Winnecke		
P_{rot} (h)	a/b	D_N (g cm^{-3})
8.15	**1.3±0.1**	**0.213**
(*Snodgrass et al.*, 2005)		
9P/Tempel		
P_{rot} (h)	a/b	D_N (g cm^{-3})
41.27±1.85	**1.572**	**0.010**
(*Lamy et al.*, 2007)		
10/Tempel		
P_{rot} (h)	a/b	D_N (g cm^{-3})
8.941±0.002	**2.0**	**0.273**
(*Knight et al.*, 2011)		
14P/Wolf		
P_{rot} (h)	a/b	D_N (g cm^{-3})
7.53±0.10	**1.7±0.1**	**0.327**
(*Snodgrass et al.*, 2005)		
17P/Holmes		
P_{rot} (h)	a/b	D_N (g cm^{-3})
6.29±0.01	**1.3±0.1**	**0.358**
(*Betzler et al.*, 2008)	(*Snodgrass et al.*, 2006)	
19P/Borrelly		
P_{rot} (h)	a/b	D_N (g cm^{-3})
26.592±0.048	**2.46±0.15**	**0.038**
(*Mueller et al.*, 2010)	(*Lamy et al.*, 1998)	
21P/Giacobini Zinner		
P_{rot} (h)	a/b	D_N (g cm^{-3})
9.5±0.2	**1.5**	**0.181**
(*Leibowitz and Brosch*. 1986)		
22P/Kopff		
P_{rot} (h)	a/b	D_N (g cm^{-3})
12.3±0.8	**1.66±0.11**	**0.120**
(*Lowry and Weissman*, 2003)		
28P/Neujmin 1		
P_{rot} (h)	a/b	D_N (g cm^{-3})
12.75±0.03	**1.51±0.07**	**0.101**
(*Delahodde et al.*, 2001)		

29P/Schwassmann-Wachmann 1		
P_{rot} (h)	a/b	D_N (g cm^{-3})
14.0	**2.6**	**0.145**
(*Meech et al.,* 1993)		
31P/Schwassmann-Wachmann 2		
P_{rot} (h)	a/b	D_N (g cm^{-3})
5.58±0.03	**1.6**	**0.560**
(*Luu and Jewitt,* 1992)		
43P/Wolf-Harrington		
P_{rot} (h)	a/b	D_N (g cm^{-3})
11.4	**3.6**	**0.302**
(*Królikowska et al.*, 2001)		
46P/Wirtanen		
P_{rot} (h)	a/b	D_N (g cm^{-3})
6.0±0.3	**1.4±0.01**	**0.424**
(*Meech, Bauer, and Hainaut*, 1997)		
47P/Ashbrook-Jackson		
P_{rot} (h)	a/b	D_N (g cm^{-3})
16±8	**1.4±0.1**	**0.060**
(*Lamy et al.*, 2011)	(*Snodgrass et al.*, 2008)	
48P/Johnson		
P_{rot} (h)	a/b	D_N (g cm^{-3})
29.00±0.04	**1.35**	**0.018**
(*Jewitt and Sheppard*, 2004)		
49P/Arend-Rigaux		
P_{rot} (h)	a/b	D_N (g cm^{-3})
9.58±0.8	**1.63**	**0.194**
(*Jewitt and Meech*, 1985)		
67P/Churyumov-Gerasimenko		
P_{rot} (h)	a/b	D_N (g cm^{-3})
12.7047±0.0011	**1.45±0.09**	**0.098**
(*Tubiana et al.*, 2011)		
70P/Kojima		
P_{rot} (h)	a/b	D_N (g cm^{-3})
22.0	**1.1**	**0.025**
(*Lamy et al.*, 2011)		
73P-C/Schwassmann-Wachmann 3		
P_{rot} (h)	a/b	D_N (g cm^{-3})
3.5	**1.8±0.3**	**1.602**
(*Toth et al.*, 2008)		
74P/Smirnova-Chernykh		
P_{rot} (h)	a/b	D_N (g cm^{-3})
20	**1.16**	**0.032**
(*Lamy et al.*, 2011)	(*Lamy et al.*, 2000)	

76P/West-Kohoutek-Ikemura		
P_{rot} (h)	a/b	D_N (g cm^{-3})
6.5±0.6	**1.14**	**0.294**
(*Lamy et al.*, 2011)	(*Lamy et al.*, 2000)	
87P/Bus		
P_{rot} (h)	a/b	D_N (g cm^{-3})
32±9	**1.35**	**0.014**
(*Lamy et al.*, 2011)	(*Lamy et al.*, 2000)	
92P/Sanguin		
P_{rot} (h)	a/b	D_N (g cm^{-3})
6.22±0.05	**1.7±0.1**	**0.479**
(*Snodgrass et al.*, 2005)		
94P/Russell 4		
P_{rot} (h)	a/b	D_N (g cm^{-3})
~ 33	**1.7±0.1**	**0.017**
(*Snodgrass et al.*, 2008)		
107P/Wilson-Harrington		
P_{rot} (h)	a/b	D_N (g cm^{-3})
6.10±0.05	**1.23±0.07**	**0.360**
(*Osip et al.*, 1995)		
110P/Hartley 3		
P_{rot} (h)	a/b	D_N (g cm^{-3})
9.4±1	**1.3**	**0.160**
(*Lamy et al.*, 2011)	(*Lamy et al.*, 2000)	
143P/Kowal Mrkos		
P_{rot} (h)	a/b	D_N (g cm^{-3})
17.21±0.10	**1.45±0.05**	**0.053**
(*Jewitt et al.*, 2003)		
147P/Kushida-Marumatsu		
P_{rot} (h)	a/b	D_N (g cm^{-3})
10.5±1	**1.53**	**0.151**
(*Lamy et al.*, 2011)	(*Lamy et al.*, 2000)	
169P/Neat		
P_{rot} (h)	a/b	D_N (g cm^{-3})
8.4096±0.00012	**1.131±0.03**	**0.174**
(*Kasuga et al.*, 2010)		
2060 Chiron		
P_{rot} (h)	a/b	D_N (g cm^{-3})
5.917813±0.000007	**1.086**	**0.338**
(*Marcialis and Buratti*, 1993)	(*Luu and Jewitt*, 1990)	
5145 Pholus		
P_{rot} (h)	a/b	D_N (g cm^{-3})
9.9832±0.0012	**1.8**	**0.197**
(*Farnham,* 2001)		

54598 Bienor		
P_{rot} (h)	a/b	D_N (g cm^{-3})
9.14±0.05	**1.995**	**0.260**
(*Ortiz et al.*, 2002)		
120061		
P_{rot} (h)	a/b	D_N (g cm^{-3})
4.99±0.01	**1.096**	**0.480**
(*Ortiz et al.*, 2006)		
8405 Asbolus		
P_{rot} (h)	a/b	D_N (g cm^{-3})
8.93±0.03	**1.66**	**0.227**
(*Davies et al.*, 1998)		
32532 Thereus		
P_{rot} (h)	a/b	D_N (g cm^{-3})
8.3±0.05	**1.159**	**0.183**
(*Ortiz et al.*, 2002)		
83982 Crantor		
P_{rot} (h)	a/b	D_N (g cm^{-3})
9.67±0.04	**1.138**	**0.133**
(*Ortiz et al.*, 2003)		
60558		
P_{rot} (h)	a/b	D_N (g cm^{-3})
26.802±0.042	**1.247**	**0.020**
(*Rousselot et al.*, 2005)		
31824 Elatus		
P_{rot} (h)	a/b	D_N (g cm^{-3})
13.41±0.04	**1.098**	**0.067**
(*Bauer et al.*, 2002)		
52872 Okyrhoe		
P_{rot} (h)	a/b	D_N (g cm^{-3})
8.3±0.3	**1.202**	**0.190**
(*Bauer et al.*, 2003)		
55576 Amycus		
P_{rot} (h)	a/b	D_N (g cm^{-3})
9.76	**1.159**	**0.133**
(*Thirouin et al.*, 2010)		
136204		
P_{rot} (h)	a/b	D_N (g cm^{-3})
8.24	**1.047**	**0.168**
(*Thirouin et al.*, 2010)		
145486		
P_{rot} (h)	a/b	D_N (g cm^{-3})
8.32	**1.127**	**0.178**
(*Thirouin et al.*, 2010)		

19981		
P_{rot} (h)	a/b	D_N (g cm^{-3})
7.71±0.02	**1.820**	**0.334**
(*Ortiz et al.*, 2003)		

136108 Haumea		
P_{rot} (h)	a/b	D_N (g cm^{-3})
3.9154±0.0002	**1.294**	**0.920**
(*Rabinowitz et al.*, 2006)		

90482 Orcus		
P_{rot} (h)	a/b	D_N (g cm^{-3})
10.08±0.01	**1.038**	**0.111**
(*Ortiz et al.*, 2006)		

50000 Quaoar		
P_{rot} (h)	a/b	D_N (g cm^{-3})
17.6788±0.0004	**1.130**	**0.039**
(*Ortiz et al.*, 2003)		

55565		
P_{rot} (h)	a/b	D_N (g cm^{-3})
8.86±0.01	**1.077**	**0.150**
(*Ortiz et al.*, 2006)		

55636		
P_{rot} (h)	a/b	D_N (g cm^{-3})
8.16	**1.038**	**0.170**
(*Thirouin et al.*, 2010)		

55637		
P_{rot} (h)	a/b	D_N (g cm^{-3})
14.382±0.001	**1.213**	**0.064**
(*Rousselot et al.*, 2005)		

20000 Varuna		
P_{rot} (h)	a/b	D_N (g cm^{-3})
6.3442±0.0002	**1.472**	**0.399**
(*Jewitt and Sheppard*, 2002)		

2003 AZ_{84}		
P_{rot} (h)	a/b	D_N (g cm^{-3})
6.76±0.01	**1.097**	**0.262**
(*Ortiz et al.*, 2006)		

84922		
P_{rot} (h)	a/b	D_N (g cm^{-3})
7.41±0.02	**1.213**	**0.241**
(*Sheppard*, 2007)		

19308		
P_{rot} (h)	a/b	D_N (g cm^{-3})
6.25±0.03	**1.117**	**0.312**
(*Hainaut et al.*, 2000)		

120348		
P_{rot} (h)	a/b	D_N (g cm^{-3})
5.85±0.01	**1.22**	**0.389**
(*Sheppard*, 2007)		
24835		
P_{rot} (h)	a/b	D_N (g cm^{-3})
4.04±0.03	**1.191**	**0.795**
(*Sheppard and Jewitt*, 2003)		
55638		
P_{rot} (h)	a/b	D_N (g cm^{-3})
9.47±0.01	**1.077**	**0.131**
(*Ortiz et al.*, 2006)		
88611		
P_{rot} (h)	a/b	D_N (g cm^{-3})
9.5055±0.0007	**1.738**	**0.210**
(*Osip et al.*, 2003)		
126154		
P_{rot} (h)	a/b	D_N (g cm^{-3})
13.25±0.2	1.2	0.075
(*Sheppard*, 2007)		
150642		
P_{rot} (h)	a/b	D_N (g cm^{-3})
4.71	**1.213**	**0.596**
(*Lacerda and Luu*, 2006)		
26308		
P_{rot} (h)	**a/b**	D_N (g cm^{-3})
7.966	**1.7**	**0.292**
(*Romanishin et al.*, 2001)		
40314		
P_{rot} (h)	a/b	D_N (g cm^{-3})
5.9529±0.001	**1.180**	**0.363**
(*Sheppard and Jewitt*, 2002)		
35671		
P_{rot} (h)	a/b	D_N (g cm^{-3})
8.84	**1.159**	**0.162**
(*Lacerda and Luu*, 2006)		
47932		
P_{rot} (h)	a/b	D_N (g cm^{-3})
8.329±0.005	**1.754**	**0.276**
(*Sheppard and Jewitt*, 2002)		
79983		
P_{rot} (h)	a/b	D_N (g cm^{-3})
6.65	**1.445**	**0.356**
(*Lacerda and Luu*, 2006)		

2003 QY_{90}		
P_{rot} (h)	a/b	D_N (g cm^{-3})
3.4±1.1	**1.368**	**1.290**
(*Kern and Elliot*, 2006)		
139775		
P_{rot} (h)	a/b	D_N (g cm^{-3})
13.7744±0.0004	**2.858**	**0.164**
(*Sheppard and Jewitt*, 2004)		
33128		
P_{rot} (h)	a/b	D_N (g cm^{-3})
6.3±0.1	**1.871**	**0.514**
(*Sheppard and Jewitt*, 2002)		
1997 CV_{29}		
P_{rot} (h)	a/b	D_N (g cm^{-3})
15.8	**1.445**	**0.063**
(*Chorney and Kavelaars*, 2004)		
2003 BG_{91}		
P_{rot} (h)	a/b	D_N (g cm^{-3})
4.2	**1.180**	**0.729**
(*Trilling and Bernstein*, 2006)		
136472 Makemake		
P_{rot} (h)	a/b	D_N (g cm^{-3})
7.65	**1.013**	**0.189**
(*Thirouin et al.*, 2010)		
42355 Typhon		
P_{rot} (h)	a/b	D_N (g cm^{-3})
9.67	**1.067**	**0.124**
(*Thirouin et al.*, 2010)		
208996		
P_{rot} (h)	a/b	D_N (g cm^{-3})
6.79	**1.067**	**0.252**
(*Thirouin et al.*, 2010)		
120132		
P_{rot} (h)	a/b	D_N (g cm^{-3})
8.54	**1.148**	**0.172**
(*Thirouin et al.*, 2010)		
174567		
P_{rot} (h)	a/b	D_N (g cm^{-3})
5.90	**1.057**	**0.331**
(*Thirouin et al.*, 2010)		
120178		
P_{rot} (h)	a/b	D_N (g cm^{-3})
4.05	**1.127**	**0.749**
(*Thirouin et al.*, 2010)		

120347		
P_{rot} (h)	a/b	D_N (g cm^{-3})
6.09	**1.028**	**0.302**
(*Thirouin et al.*, 2010)		
144897		
P_{rot} (h)	a/b	D_N (g cm^{-3})
5.68	**1.076**	**0.364**
(*Thirouin et al.*, 2010)		
145452		
P_{rot} (h)	a/b	D_N (g cm^{-3})
5.62	**1.038**	**0.358**
(*Thirouin et al.*, 2010)		
2005 CB_{29}		
P_{rot} (h)	a/b	D_N (g cm^{-3})
6.76	**1.127**	**0.269**
(*Thirouin et al.*, 2010)		
145453		
P_{rot} (h)	a/b	D_N (g cm^{-3})
7.87	**1.057**	**0.186**
(*Thirouin et al.*, 2010)		

Matlab Code used for generating Figure 6:

```
clear; close all
x = [1.44 1.18 1.3 1.572 2.0 1.7 1.3 2.46 1.5 1.66 1.51 2.6 1.6 3.6 1.4
1.40 1.35 1.63 1.45 1.1 1.8 1.16 1.14 1.35 1.7 1.7 1.23 1.3 1.49 1.53
1.31];
y = [11.083 7.20 8.15 41.27 8.941 7.53 6.29 26.592 9.5 12.3 12.75 14.0 5.58
11.4 6.0 16.0 29.0 9.58 12.047 22.0 3.5 20.0 6.5 32.0 6.22 33.0 6.10 9.4
17.21 10.5 8.4096];
%JFC data where y is the rotation period and x is a/b.
x2 = [1.086 1.8 1.995 1.096 1.66 1.159 1.138 1.247 1.098 1.202 1.159 1.047
1.127];
y2 = [5.917813 9.98232 4.57 4.99 8.93 4.15 9.67 26.802 13.41 8.3 9.76 8.24
8.32];
%Centaur data.
x3 = [1.820 1.294 1.038 1.130 1.077 1.038 1.213 1.472 1.097 1.213 1.117
1.22 1.191 1.077 1.738 1.2 1.213 1.7 1.180 1.159 1.754 1.445 1.368 2.858
1.871 1.445 1.180 1.013 1.067 1.067 1.148 1.057 1.127 1.028 1.076 1.038
1.127 1.057];
y3 = [7.71 3.9154 10.08 17.6788 8.86 8.16 14.382 6.3442 6.76 7.41 6.25 5.85
4.04 9.47 4.7526 13.25 4.71 3.983 5.9529 8.84 8.329 6.65 3.4 13.7744 4.9
15.8 4.2 7.65 9.67 6.79 8.54 5.90 4.05 6.09 5.68 5.62 6.76 7.87];
%KBOs data.
A=log10(y);
B=log10(y2);
C=log10(y3);
figure, plot(x,A,'co','markerfacecolor','c');hold on;
plot(x2,B,'g^','markerfacecolor','g'); hold on;
```

```
plot(x3,C,'rs','markerfacecolor','r');
%Cyan filled circles = JFCs, gree filled triangles = Centaurs, Blue filled
squares = KBOs
set(gca,'YTick',0.25:0.25:1.75);
set(gca,'XTick',1.0:0.5:4.0);
%Changing axis ranges. Y is 0.25->1.75 in steps of 0.25. X is 0.5->4 in
steps of 0.5.
h=legend('Jupiter Family Comets','Centaurs','Kuiper Belt
Objects','Location','NW');
set(h,'FontWeight','bold','FontSize',14);
xlabel('Axis Ratio [a/b]','FontWeight','bold','FontSize',14);
ylabel('Log of Rotational Period [h]','FontWeight','bold','FontSize',14);
title('Axis Ratio Vs. Log of Rotational Period',
'FontWeight','bold','FontSize',18);%bold title
axis([1.0 4.0 0.25 1.75]);

X = 1.0:0.1:4;
p = 2.00;
Y = (3.3/sqrt(p))*sqrt(X);%equation for critical rot
M = log10(Y);
plot(X,M,'b:');
text(3.9,0.64,'\color{blue}2.00','FontWeight','bold','FontSize',14)%text
label for line
hold on

p = 0.6;
Y = (3.3/sqrt(p))*sqrt(X);
M = log10(Y);
plot(X,M,'b:');
text(3.9,0.9,'\color{blue}0.60','FontWeight','bold','FontSize',14)
hold on

p = 0.2;
Y = (3.3/sqrt(p))*sqrt(X);
M = log10(Y);
plot(X,M,'b:');
text(3.9,1.14,'\color{blue}0.20','FontWeight','bold','FontSize',14)
hold on
p = 0.06;
Y = (3.3/sqrt(p))*sqrt(X);
M = log10(Y);
plot(X,M,'b:');
text(3.9,1.4,'\color{blue}0.06','FontWeight','bold','FontSize',14)
hold on
p = 0.02;
Y = (3.3/sqrt(p))*sqrt(X);
M = log10(Y);
plot(X,M,'b:');
text(3.9,1.64,'\color{blue}0.02','FontWeight','bold','FontSize',14)
text(3.7,1.70,'\color{blue}\rho_b (g \itcm^{-
3})','FontWeight','bold','FontSize',14)%text label for Units
```

REFERENCES

Bauer J. M.; Meech K. J.; Fernández Y. R., Farnham T. L.; Roush T. L. (2002) Observations of the Centaur 1999 UG_5: Evidence of a Unique Outer Solar System Surface. *The Publications of the Astronomical Society of the Pacific*, 114, 802, pp. 1309-1321

Bauer J. M., Meech K. J., Fernández Y. R., Pittichova J., Hainaut O. R., Boehnhardt H., Delsanti A. C. (2003) Physical survey of 24 Centaurs with visible photometry. *Icarus*, 166, 1, pp. 195-211

Betzler A. S., Ferreira D. H., Ribeiro D. S., Tárcio H., Novaes A. B., and Celeden J. H. Q. (2008) The Synodic Rotation Period of Comet 17P7Holmes %C ALPO. *Journal of the Association of Lunar & Planetary Observers*, The Strolling Astronomer, 50, 3, pp. 23-26

Chorney N. and Kavelaars J.J. (2004) A rotational light curve for the Kuiper belt object 1997 CV_{29}. *Icarus*, 167, 1, pp. 220-224

Davies J. K., McBride N., Ellison S. L., Green S. F., and Ballantyne D. R. (1998) Visible and Infrared Photometry of Six Centaurs. *Icarus*, 134, 2, pp. 213-227

Delahodde C. E., Meech K. J., Hainaut O. R., and Dotto E. (2001) Detailed phase function of comet 28P/Neujmin 1. *Astronomy and Astrophysics*, 376, pp. 672-685

Duncan M. and Levison H. F. (1997) A scattered comet disk and the origin of Jupiter-family comets. *Science*, 276, pp.1670-1672.

Duncan M., Levison H., and Dones L. (2004) Dynamical Evolution of Ecliptic Comets. In *Comets II* (M C. Festou et al., eds), pp. 193-204. Univ. of Arizona, Tucson

Farnham T. L. (2001) The Rotation Axis of the Centaur 5145 Pholus. *Icarus*, 152, 2, pp. 238-245

Hainaut, O. R., Delahodde C. E., Boehnhardt H., Dotto E., Barucci M. A., Meech K. J., Bauer J. M., West R. M., and Doressoundiram A. (2000) *Astronomy and Astrophysics*, 356, pp. 1076-1088

Harmon J. K., Nolan M. C., Ostro S. J., and Campbell D. B. (2004) Radar Studies of Comet Nuclei and Comae. In *Comets II* (M. C. Festou et al., eds), pp. 265-279. Univ. of Arizona, Tucson

Harmon J. K. and Nolan M. C. (2005) Radar observations of Comet 2P/Encke during the 2003 apparition. *Icarus*, 176, pp. 175-183

Harmon J. K., Nolan M. C., Howell E. S., Giorgini J. D., and Taylor P. A. (2011) Radar Observations of Comet 103P/Hartley 2. *The Astrophysical Journal Letters*, 734, 1, L2

Holsapple K. A. (2003) Could fast rotator asteroids be rubble piles? In *Lunar and Planetary Science XXXIV*, Abstract #1792, Lunar and Planetary Institute, Houston

Jewitt D. C. (2004) From Cradle To Grave: The Rise and Demise of the Comets. In *Comets II* (M. C. Festou et al., eds), pp. 659-676. Univ. of Arizona, Tucson

Jewitt D. C. and Sheppard S. (2004) The Nucleus of Comet 48P/Johnson. *The Astronomical Journal,* 127, 3, pp.1784-1790

Jewitt D., Sheppard S., and Fernández Y. (2003) 143P/Kowal-Mrkos and the Shapes of Cometary Nuclei. *The Astronomical Journal,* 125, 6, pp.3366-3377

Jewitt D. and Sheppard S.S. (2002) Physical Properties of Trans-Neptunian Object (20000) Varuna *The Astronomical Journal,* 123, 4, pp.2110-2120

Jewitt D. C. and Meech K. J. (1985) Rotation of the nucleus of Comet p/Arend-Rigaux. *Icarus*, 64, pp. 329-335

Kasuga T., Balam D. D., and Wiegert P. A. (2010) Comet 169P/NEAT (=2002 EX_{12}): The Parent Body of the α- Capricornid Meteoroid Stream. *The Astronomical Journal,* 140, 6, pp.1806-1813

Keller H. U., Britt D., Buratti B. J., and Thomas N. (2004) In Situ Observation of Cometary Nuclei. In *Comets II* (M. C. Festou et al., eds), pp. 211-222. Univ. of Arizona, Tucson

Kern S. D. and Elliot J. L. (2006) Discovery and characteristics of the Kuiper Belt binary 2003 QY_{90}. *Icarus*, 183, 1, pp. 179-185

Knight M. M., Farnham T. L., Schleicher D. G., and Schwieterman E. W. (2011) The Increasing rotation period of comet 10P/Tempel 2. *The Astronomical Journal*, 141, 2

Królikowska M., Sitarski G., and Szutowicz S. (2001) Forced precession models for six erratic comets. *Astronomy and Astrophysics*, 368, pp. 676-688

Lacerda P. and Luu J. (2006) Analysis of the rotational properties of Kuiper Belt Objects. *The Astronomical Journal*, 131, pp. 2314-2326

Lamy P. L., Toth I., and, Weaver H. A. (1998) Hubble Space Telescope observations of the nucleus and inner coma of comet 19P/1904 Y2 (Borrelly). *Astronomy and Astrophysics*, 337, pp. 945-954

Lamy P.L., Toth I., Weaver H. A., Delahodde C. Jorda L., and A 'Hearn M. F. (2000) The nucleus of 13 short-period comets *American Astronomical Society*, DPS meeting #32, #36.04 and *Bulletin of the American Astronomical Society*, 32, p. 1061, Abstract

Lamy P. L., Toth I., Fernandez Y. R., Weaver H. A. (2004) The Sizes, Shapes, Albedos, and Colors of Cometary Nuclei. In *Comets II* (M. C. Festou et al., eds), pp. 223-264. Univ. of Arizona, Tucson

Lamy P.L., Toth I., A 'Hearn M. F., Weaver H. A., and Jorda L. (2007) Rotational state of the nucleus of Comet 9P/Tempel 1: Results from the Hubble Space Telescope observations in 2004. *Icarus,* 187, 1, pp. 132-143

Lamy P.L., Toth I., Weaver H. A., A 'Hearn M. F., and Jorda L. (2011) Properties of the nuclei and Comae of 10 ecliptic comets from the Hubble Space Telescope multi-orbit observations. *Monthly Notices of the Royal Astronomical Society*, 412, 3, pp. 1573-1590

Leibowitz E. K. and Brosch N. (1986) Periodic photometric variations in the near- nucleus zone of P/Giacobini-Zinner. *Icarus*, 68, pp. 430-441.

Levison H. F., Duncan M. J. (1994) The long-term dynamical behaviour of short-period comets. *Icarus*, 108, pp. 18-36.

Levison Duncan 1996 From the Kuiper Belt to Jupiter-Family Comets: The Spatial Distribution of Ecliptic Comets

Lomb N. R. (1976) Least-squares frequency analysis of unequally spaced data. *Astrophysics and Space Science*, 39, pp. 447-462.

Lowry S. C. and Weissman P.R. (2003) CCD observations of distant comets from Palomar and Steward Observatories. *Icarus*, 164, 2, pp. 492-503

Lowry S. C. and Weissman P.R. (2007) Rotation and color properties of the nucleus of Comet 2P/Encke. *Icarus*, 188, 1, pp. 212-223

Lowry S. C., Fitzsimmons A., Lamy P., Weissman P. (2008) Kuiper Belt Objects in the Planetary Region: The Jupiter-Family Comets. In *The Solar System Beyond Neptune* (M. A. Barucci et al., eds.), pp. 397-410. Univ. of Arizona, Tucson

Luu J. X. and Jewitt D. C. (1990) Cometary activity in 2060 Chiron. *Astronomical Journal*, 100, 6, pp. 913-932

Luu J.X. and Jewitt D. C. (1992) Near-aphelion CCD photometry of Comet P/S Schwassmann-Wachmann 2. *Astronomical Journal*, 104, 6, pp. 2243-2249

Marcialis R. L. and Buratti B. J. (1993) CCD photometry of 2060 Chiron in 1985 and 1991. *Icarus*, 104, 2, pp. 234-243

Meech K. J., Belton M. J. S., Mueller B. E. A., Dicksion M. W., and Li H. R. (1993) Nucleus properties Of P/Schwassmann-Wachmann 1. *Astronomical Journal*, 106, 3, pp. 1222-1236

Meech K. J., Bauer J. M., and Hainaut O. R. (1997) Rotation of comet 46P/Wirtanen. *Astronomy and Astrophysics*, 326, pp. 1268-1276

Meech K. J. and Svoreň J. (2004) Using Cometary Activity to Trace the Physical and Chemical Evolution of Cometary Nuclei. In *Comets II* (M. C. Festou et al., eds), pp. 317-335. Univ. of Arizona, Tucson

Morbidelli A. and Brown M. E. (2004) The Kuiper Belt and the Primordial Evolution of the Solar System. In *Comets II* (M. C. Festou et al., eds), pp. 175-191. Univ. of Arizona, Tucson

Mueller B. E. A., Samarasinha N. H., Rauer H., and Helbert J. (2010) Determination of a precise Rotation period for the Deep Space 1 target, Comet 19P/Borrelly. *Icarus*, 209, 2, pp. 745-752

Ortiz J. L., Baumont S., Gutiérrez P. J., and Roos-Serote M. (2002) Lightcurves of Centaurs 2000 QC_{243} and 2001 PT_{13}. *Astronomy and Astrophysics*, 388, pp.661-666

Ortiz J. L., Gutiérrez P. J., Casanova V., and Sota A. (2003) A study of short term rotational variability in TNOs and Centaurs from Sierra Nevada Observatory. *Astronomy and Astrophysics*, 407, pp. 1149-1155

Ortiz J. L., Gutiérrez P. J., Sota A., Casanova V., and Teixeira V.R. (2003) Rotational brightness Variations in Trans-Neptuninan Object 50000 Quaoar. *Astronomy and Astrophysics*, 409, 3, pp. 1131-1144

Ortiz J. L., Gutiérrez P. J., Santos-Sanz P., Casanova V., and Sota A. (2006) Short-term rotational Variability of eight KBOs from Sierra Nevada Observatory. *Astronomy and Astrophysics*, 447, 3, pp. L13-L16

Osip D. J., Kern S. D., and Elliot J.L. (2003) Physical Characterization of the Binary Edgeworth-Kuiper Belt Object 2001 QT_{297}. *Earth, Moon, and Planets*, 92, 1, pp.409-421

Osip D., Campins H., and Schleicher D. G. (1995) The rotation state of 4015 Wilson-Harrington: Revisiting origins for the near-Earth asteroids. *Icarus*, 114, 2, pp. 423-426

Pravec P. and Harris A. W. (2000) Fast and slow rotation of asteroids. *Icarus*, 148, pp. 12-20

Rabinowitz D. L., Barkume K., Brown M. E., Roe H., Schwartz M.,Tourtellotte S., and Trujillo C. (2006) Photometric Observations Constraining the Size, Shape, and Albedo of 2003 EL61, a Rapidly Rotating, Pluto-sized Object in the Kuiper Belt. *The Astrophysical Journal,* 639, 2, pp. 1238-1251.

Romanishin W., Tegler S.C., Rettig T. W., Consolmagno G., and Botthof B. (2001) SM165: A large Kuiper belt object with an irregular shape. *Proceedings of the National Academy of Science*, 98, 21, pp. 11863-11866

Rousselot P., Petit J. M., Poulet F., and Sergeev A. (2005) Photometric study of Centaur (60558) 2000 EC_{98} and trans-neptunian object (55637) 2002 UX_{25} at different phase angles. *Icarus*, 176, 2, pp. 478-491

Samarasinha N. H., Mueller B. E. A., Belton M. J. S., Jorda L. (2004) Rotation of Cometary Nuclei. In *Comets II* (M. C. Festou et al., eds), pp. 281-299. Univ. of Arizona, Tucson

Sheppard S. S., Lacerda P., Ortiz J. L. (2008) Photometric Lightcurves of Transneptunian Objects and Centaurs: Rotation, Shapes, and Densities. In *The Solar System Beyond Neptune* (M. A. Barucci et al., eds.), pp. 129-142. Univ. of Arizona, Tucson

Sheppard S. S. (2007) Light Curves of Dwarf Plutonian Planets and other Large Kuiper Belt Objects: Their Rotations, Phase Functions, and Absolute Magnitudes. *The Astronomical Journal*, 134, 2, pp. 787-798

Sheppard S. S. and Jewitt D. C. (2004) Extreme Kuiper Belt Object 2001 QG_{298} and the Fraction of Contact Binaries. *The Astronomical Journal*, 127, 5, pp. 3023-3033

Sheppard S. S. and Jewitt D. C. (2003) Hawaii Kuiper Belt Variability Project: An Update. *Earth, Moon, and Planets*, 92, 1, pp. 207-219

Sheppard S. S. and Jewitt D. C. (2002) Time-resolved Photometry of Kuiper Belt Objects: Rotation, Shapes, and Phase Functions. *The Astronomical Journal*, 124, 3, pp. 1757-1775

Snodgrass C., Fitzsimmons A., and Lowry S. C. (2005) The nuclei of comets 7P/Pons-Winnecke, 14P/Wolf and 92P/Sanguin. *Astronomy and Astrophysics*, 444, 1, pp.287-295

Snodgrass C., Lowry S. C., and Fitzsimmons A. (2006) Photometry of cometary nuclei: rotation states, Colours and a comparison with Kuiper Belt Objects. *Monthly Notices of the Royal Astronomical Society*, 373, 4, pp. 1590-1602

Snodgrass C. (2006) Forms and rotational states of the nuclei of ecliptic comets. Ph.D. thesis, Queen's Univ. Belfast

Snodgrass C., Lowry S. C., and Fitzsimmons A., (2008) Optical observation of 23 distant Jupiter Comets, including 36P/Whipple at multiple phase angles. *Monthly Notices of the Royal Astronomical Society*, 412, 3, pp. 1573-1590

Thirouin A., Ortiz, J. L., Duffard R., Santos-Sanz, P., Aceituno, F. J., and Morales, N. (2010) Short-term variability of a sample of 29 trans-Neptunian objects and Centaurs. *Astronomy and Astrophysics*, 522, A93

Toth I., Lamy P.L., Weaver H. A., Noll K. S., and Mutchler M.J. (2008) Hubble Space Telescope Observations of Fragment C of the Split Comet 73P/Schwassmann-Wachmann 3 in 2001 and 2006. *American Astronomical Society*, DPS meeting #40, #5.08 and *Bulletin of the American Astronomical Society*, 40, p. 394, Abstract

Trilling D. E. and Bernstein G. M. (2006) Light Curves of 20-100 km Kuiper Belt Objects Using the Hubble Space Telescope. *The Astronomical Journal,* 131, 2, pp. 1149-1162.

Tubiana C., Böhnhardt H., Agarwal J., Drahus M., Barrera L., and Ortiz J. L. (2011) 67P/Churyumov-Gerasimenko at large heliocentric distance. *Astronomy & Astrophysics*, 527

Volk K., Malhotra R. (2008) The Scattered Disk as the Source of the Jupiter Family Comets. *The Astrophysical Journal,* 385, 2, pp. 737-756.

Weidenschilling S. J. (2004) From icy grains to comets. In *Comets II* (M. C. Festou et al., eds), pp. 97-104. Univ. of Arizona, Tucson

Weissman P. R., Asphaug E., and Lowry S. C. (2004) Structure and Density of Cometary Nuclei. In *Comets II* (M. C. Festou et al., eds), pp. 337-357. Univ. of Arizona, Tucson

Online Resources:

[1] Wikipedia, 2009. *Prolate Spheroid*. [image online]. Available at: <http://upload.wikimedia.org/wikipedia/commons/8/88/ProlateSpheroid.png> [Accessed 25 January 2012]

[2] Jet Propulsion Laboratory, National Aeronautics and Space Administration, 1994. *Hubble's Panoramic Picture of Comet Shoemaker-Levy 9*. [image online]. Available at: < http://www2.jpl.nasa.gov/sl9/gif/hst2.gif > [Accessed 06 February 2012]

[3] National Aeronautics and Space Administration, Jet Propulsion Laboratory, 2005. *Enki Catena Crater Chain on Ganymede.* [image online]. Available at: <http://neo.jpl.nasa.gov/images/ganymede1.jpg > [Accessed 06 February 2012]

[4] National Aeronautics and Space Administration, Jet Propulsion Laboratory, Small Body Data Base, 2012. Orbit Diagram of 67P/Churyumov-Gerasimenko. [image online]. Available at: < http://ssd.jpl.nasa.gov/sbdb.cgi?sstr=67P;orb=1;cov=0;log=0;cad=0#orb> [Accessed 06 February 2012]

[5] National Aeronautics and Space Administration, Jet Propulsion Laboratory, Small Body Data Base, 2012. Orbit Diagram of 31824 Elatus. [image online]. Available at: < http://ssd.jpl.nasa.gov/sbdb.cgi?sstr=Elatus;orb=1;cov=0;log=0;cad=0#orb> [Accessed 06 February 2012]

[6] National Aeronautics and Space Administration, Jet Propulsion Laboratory, Small Body Data Base, 2012. Orbit Diagram of 136108 Haumea. [image online]. Available at: < http://ssd.jpl.nasa.gov/sbdb.cgi?sstr=Haumea;orb=1;cov=0;log=0;cad=0#orb > [Accessed 06 February 2012]

National Space Science Data Center /National Aeronautics and Space Administration, 2012. *ISEE 3* [online] Available at: <http://nssdc.gsfc.nasa.gov/nmc/spacecraftDisplay.do?id=1978-079A> [Accessed 06 February 2012]

European Space Agency / Science Programme, 2003. *Giotto* [online] Available at: <http://sci.esa.int/science-e/www/object/index.cfm?fobjectid=31718 > [Accessed 06 February 2012]

National Space Science Data Center /National Aeronautics and Space Administration, 2012. *Deep Space 1* [online] Available at: <http://nssdc.gsfc.nasa.gov/nmc/spacecraftDisplay.do?id=1998-061A > [Accessed 06 February 2012]

National Space Science Data Center /National Aeronautics and Space Administration, 2012. *Stardust and Stardust / NExT* [online] Available at: <http://nssdc.gsfc.nasa.gov/nmc/spacecraftDisplay.do?id=1999-003A > [Accessed 06 February 2012]

National Space Science Data Center /National Aeronautics and Space Administration, 2012. *Deep Impact / EPOXI* [online] Available at: <http://nssdc.gsfc.nasa.gov/nmc/spacecraftDisplay.do?id=2005-001A > [Accessed 06 February 2012]

National Space Science Data Center /National Aeronautics and Space Administration, 2012. *Rosetta* [online] Available at: <http://nssdc.gsfc.nasa.gov/nmc/spacecraftDisplay.do?id=2004-006A > [Accessed 06 February 2012]